OPEN ACCESS
IOP Publishing
Nanotechnology
Nanotechnology **32** (2021) 475202 (7pp)
https://doi.org/10.1088/1361-6528/ac1a93

Fabrication of plasmonic structures with well-controlled nanometric features: a comparison between lift-off and ion beam etching

B Abasahl[1], C Santschi, T V Raziman[2] and O J F Martin

Nanophotonics and Metrology Laboratory, Swiss Federal Insititute of Technology Lausanne (EPFL), CH-1015 Lausanne, Switzerland

E-mail: olivier.martin@epfl.ch

Received 5 July 2021, revised 13 July 2021
Accepted for publication 4 August 2021
Published 31 August 2021

Abstract

After providing a detailed overview of nanofabrication techniques for plasmonics, we discuss in detail two different approaches for the fabrication of metallic nanostructures based on e-beam lithography. The first approach relies on a negative e-beam resist, followed by ion beam milling, while the second uses a positive e-beam resist and lift-off. Overall, ion beam etching provides smaller and more regular features including tiny gaps between sub-parts, that can be controlled down to about 10 nm. In the lift-off process, the metal atoms are deposited within the resist mask and can diffuse on the substrate, giving rise to the formation of nanoclusters that render the nanostructure outline slightly fuzzy. Scattering cross sections computed for both approaches highlight some spectral differences, which are especially visible for structures that support complex resonances, such as Fano resonances. Both techniques can produce useful nanostructures and the results reported therein should guide the researcher to choose the best suited approach for a given application, depending on the available technology.

Keywords: nanotechnology, plasmonics, ion beam etching, lift-off, electron beam lithography, nanofabrication, nanostructures

(Some figures may appear in colour only in the online journal)

The shape of a nanostructure determines its optical response. This is especially true for plasmonics, the resonant excitation of free electrons in coinage metals [1]. Indeed, the smallest geometrical features on the outline of a nanostructure can, at a given frequency, localize the free electrons and pinpoint a specific plasmonic mode [2]. This poses a serious nanotechnology challenge: the slightest geometry variation can significantly modify the optical response of the structure. These modifications are apparent not only in the far-field spectrum, but also in the near-field enhancement produced by the nanostructure. An iconic example being the strong field enhancement localized in a pair of plasmonic nanostructures, such as a plasmonic dipole antenna. The exact gap dimensions control both the antenna resonance wavelength and its near-field enhancement [3]. Consequently, there have been significant efforts to produce particularly small gaps, to exploit extremely strong field enhancement [4–7], or to study the onset of interesting effects such as non-locality or electron tunneling between both metallic parts [8, 9].

[1] Present address: Münster Nanofabrication Facility, Busso-Peus-Str. 10, D-48149 Münster, Germany.
[2] Present address: Department of Applied Physics and Institute for Photonic Integration, Eindhoven University of Technology, 5600 MB Eindhoven, The Netherlands.

Original content from this work may be used under the terms of the Creative Commons Attribution 4.0 licence. Any further distribution of this work must maintain attribution to the author(s) and the title of the work, journal citation and DOI.

 © 2021 The Author(s). Published by IOP Publishing Ltd Printed in the UK

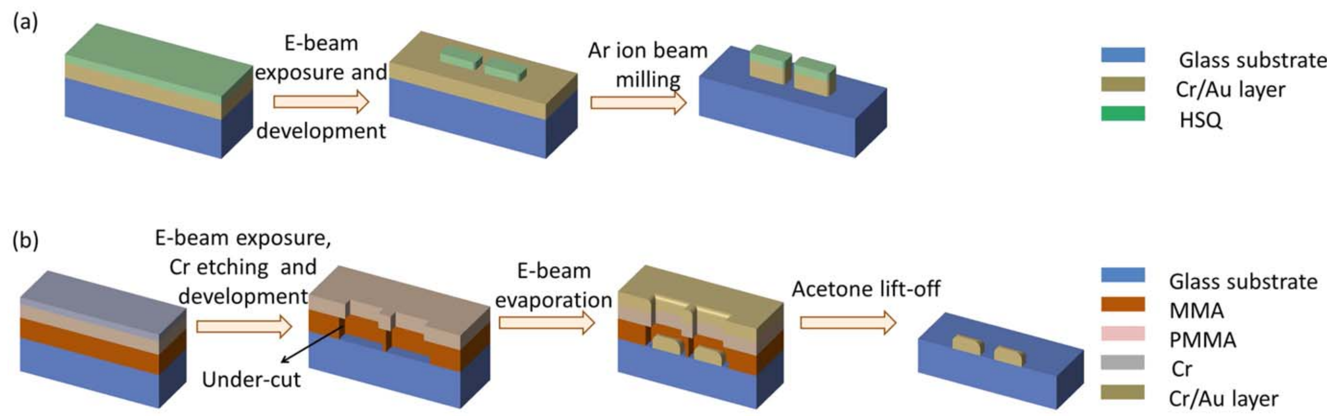

Figure 1. The different steps required for the fabrication of plasmonic nanostructures using (a) ion beam milling or (b) lift-off. See text for details.

Here, we focus on the controlled fabrication of nanostructures using a so-called top-down approach. Alternative bottom-up approaches, akin to synthesis, are also extensively used in plasmonics, although they do not provide full control on the structure shape [10–13]. Overall, the accurate fabrication of plasmonic nanostructures requires a technology that can reliably control the dimensions well below 100 nm, typically in the 10 nm range and better. Following the pioneering work of Craighead and Niklasson [14], it was soon recognized that electron beam (e-beam) lithography was the tool of choice to address this challenge [15–31]. Alternative top-down approaches based on light beams and their interference [32–34], nanoimprint and related techniques [35–40], or colloidal lithography [41–45], have also been utilized to fabricate plasmonic nanostructures in a controlled way. Focused ion beam milling deserves also a special mention, as it allows full design freedom [46–51], and has been recently used to produce beautiful plasmonic nanostructures from single monocrystalline flakes [52–57].

Once a structure has been defined with e-beam lithography in the e-beam resist, this pattern must be transferred to the plasmonic metal—usually gold, although other plasmonic materials can be used [58–62]. For the vast majority of published works, including those previously cited, this transfer is performed using a lift-off process as described below. However, recently, we have seen reports on the utilization of ion beam etching for that task [63, 64]. Unfortunately, to the best of our knowledge, there does not exist a careful comparison of both approaches and the aim of this letter is to address this shortcoming by comparing the same plasmonic nanostructures that have been realized by lift-off or dry etching. By providing the details for both recipes, we hope that this work can serve as useful reference for those wishing to undertake the fabrication of plasmonic nanostructures.

Both nanotechnologies to transfer the exposed e-beam resist into the plasmonic metal are described in figure 1. For *ion beam etching*—also called dry etching—the steps are as follows, see figure 1(a): (1) the glass substrate is cleaned with oxygen plasma at 200 W for 5 min (PVA Tepla GIGAbatch); (2) a bilayer of Cr (1 nm) and Au (40 nm) is deposited using e-beam evaporation (Leybold Optics, LAB 600); (3) the sample is cleaned in a solution of tetramethyl ammonium hydroxide (MF-CD-26) for 30 s, then rinsed in distilled (DI) water until the resistivity is higher than 12 MΩ, and dried with a nitrogen gun; (4) the sample is baked on a hotplate (Prazitherm) for 5 min at 180 °C in order to remove residuals of loosely bound water; (5) to etch a 40 nm of Au, a 40 nm layer of hydrogen silsesquioxane (HSQ, DuPont) is spun coated onto the sample (no post baking is required); (6) the sample is exposed to the e-beam of 100 keV electron energy with the doses of 1600–4000 μC cm^{-2}; (7) right after the exposure, the sample is developed in MF-CD-26 (Rhom and Haas Electronic Materials LLC) for 1 min with gentle rotation of the petri dish, followed by rinsing in DI water and drying with a nitrogen gun; (8) the sample is exposed to low-energy argon ion beam in an ion beam etcher (IBE, Veeco Nexus IBE 350) for a total of 25 s etching time in successive cycles of 5 s followed by 30 s of temperature equalization, with the current perpendicular to the sample; the etching is finished by a last step of 5 s where the sample has a 5° inclination with respect to the current to decrease the effect of material redeposition on the sides of the structure. The exposed HSQ, which is partly consumed during etching, remains on top of the structure. Usually this thin glass-like layer does not perturb the optical response; it can however be removed by first depositing a thin sacrificial Cr layer between Au and HSQ and using a Cr etch at the end of the process to remove Cr and detach the remaining HSQ (in that case, Cr cannot be used as adhesion layer and must be replaced, e.g. with Ti).

For *lift-off* the steps are—see figure 1(b): (1) the surface of the glass substrate is cleaned and activated with oxygen plasma at 200 W for 5 min (PVA Tepla GIGAbatch); (2) the sample is pre-baked on a hotplate (Prazitherm) for 5 min at 180 °C in order to remove residuals of loosely bound water; (3) after cooling down to room temperature for 1 min, a bilayer of methylmethacrylate (MMA, 8.5 EL6, 100 Da, Microresist Technology GmbH) of 120 nm and polymethylmethacrylate (PMMA, A2, 950 kDa, Microresist Technology GmbH) of 60 nm is spun coated onto the sample (ATMsse OPTIspin SB20), after each layer the sample is baked on a hotplate (Prazitherm) for 5 min at 180 °C, above

the glass transition temperature, in order to evaporate the solvent from the resist, solidify the polymer and evacuate air bubbles; (4) a 20 nm layer of Cr is evaporated onto the sample in order to compensate the lack of substrate conductivity during the e-beam exposure and to provide a reflecting reference for the interferometric height inspection; (5) the sample is exposed to the e-beam of 100 keV electron energy with the doses of 600–900 μC cm^{-2}; (6) after the exposure, the sacrificial Cr layer is etched in a fresh mixture of cerium ammonium nitride and perchloric acid (10.9%:4.25%:84:85% water, TechniETCH Cr01 MicroChemicals), normally 1 min is sufficient to totally remove the Cr layer although a longer time up to 5 min does not seem to damage the resist; (7) the sample is developed in 1:3 methyl isobutyl ketone:isopropanol (MIBK:IPA) for 1 min with rotational movement in order to avoid diffusion limited removal and to ensure total removal of the exposed resist, afterwards the sample is rinsed in IPA for 30 s to wash away the developer and finally dried with a gentle nitrogen flow; (8) in order to remove the resist residuals in the developed regions and to activate the surface, the sample is treated with a soft oxygen plasma at 120 W for 8 s (Oxford PRS900); (9) a bilayer of Cr (1 nm) and Au (40 nm) is deposited onto the sample using an e-beam evaporator (Leybold Optics LAB 600). (10) The lift-off process is performed in an acetone bath and typically lasts overnight or, depending on the nanostructures sizes and density, even longer. Afterward the sample is cleaned with IPA and dried with a nitrogen gun.

A few remarks can be made at this stage: the main differences between both recipes are (a) the order of the different steps, with the plasmonic metal being deposited at the beginning of the process for ion beam etching and at the end for lift-off, and (b) the utilization of a negative resist (HSQ) for ion etching and positive resists (MMA/PMMA) for lift-off. During development, the exposed negative resist remains and serves as hard mask for the subsequent ion beam etching step; on the other hand, the exposed positive resist disappears, revealing on the substrate the locations where the nanostructures will be formed. We use Cr as adhesion layer for Au on glass; Ti or a monolayer of mercaptosilane are also possible and—in any case—this adhesion layer should be extremely thin to avoid perturbing the plasmon resonances [65, 66]. Other metals, like Ag or Al for example, benefit from using a thin silver oxide seed layer [67]. The oxygen plasma treatment used to activate the surface removes adsorbed organic compounds from the surface efficiently. In addition, this bombardment with energetic particles creates chemically active free radicals on the surface. Upon reaction with water molecules from ambient air, reactive hydroxyl radicals are formed at the substrate/air interface, which increase the chemical reaction potential of the surface, leading to an enhanced wettability and a better adhesion of the resist [68, 69]. For the lift-off process, it is important to use an evaporator with a long distance between the metal source and the sample, to have an atom flow as collimated as possible reaching the sample. This will avoid metal deposition on the e-beam resist sidewalls, which would make the lift-off imprecise with the metal film torn, as illustrated in figure 2. In

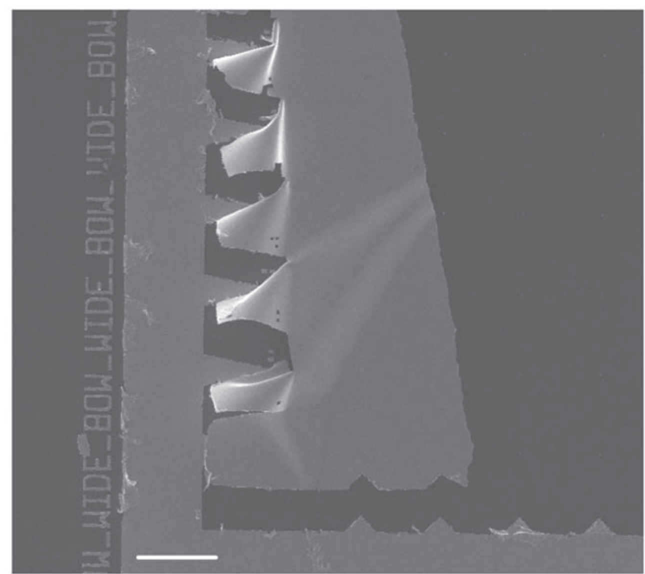

Figure 2. Illustration of a poor lift-off by lack of double e-beam resist layer. Scale bar 10 μm.

that context, the utilization of a two-layer e-beam resist is very important: the bottom layer is chosen such that it is more exposed than the top layer, creating an undercut that will prevent the deposition of a continuous metal film that would not lift-off properly, figure 2. Here, we are using MMA and PMMA as double layer; two layers of PMMA with different molecular weights can also be used (e.g. 495 kDa for the bottom layer and 950 kDa for the top layer). Besides ion beam etching, reactive ion etching is broadly used in the semiconductor industry [70, 71]. While it can etch efficiently most semiconductors and a few metals such as Al, Ti, Pt and Cr, unfortunately reactive ion etching cannot etch Au or Ag.

Figure 3 shows the same plasmonic structures realized with ion beam milling (left column) and lift-off (right column). A diversity of plasmonic nanostructures have been chosen to illustrate the performances of both recipes for different situations: (a) a simple dipole antenna, (b) a ring, (c) a heptamer, (d) a dolmen, (e) a doughnut and (f) a spiral. Comparing both columns, one clearly observes that overall the ion beam etching produces nanostructures that are much better defined than those realized with lift-off. The outline is clearer with etching, while the structures produced by lift-off appear rather distorted. This is caused by the double layer e-beam resist undercut, which leaves ample space for the adatoms to diffuse on the substrate before they become constrained by the bottom e-beam resist layer walls. This diffusion of metal clusters leads to a fuzzy nanostructure outline. Ion beam etching also enables the definition of smaller gaps between adjacent nanostructures; this is clearly visible for the dipole antenna, for which a sub-10 nm gap can be realized with ion etching, figure 3(a). Note also that in this case the gap is very straight throughout, while lift-off produces a pair of ellipsoids that recess at one point. The small gaps achieved by the ion beam etching approach are much more reproducible and the yield is significantly higher compared to lift-off, since HSQ has a high yield and a very good resolution,

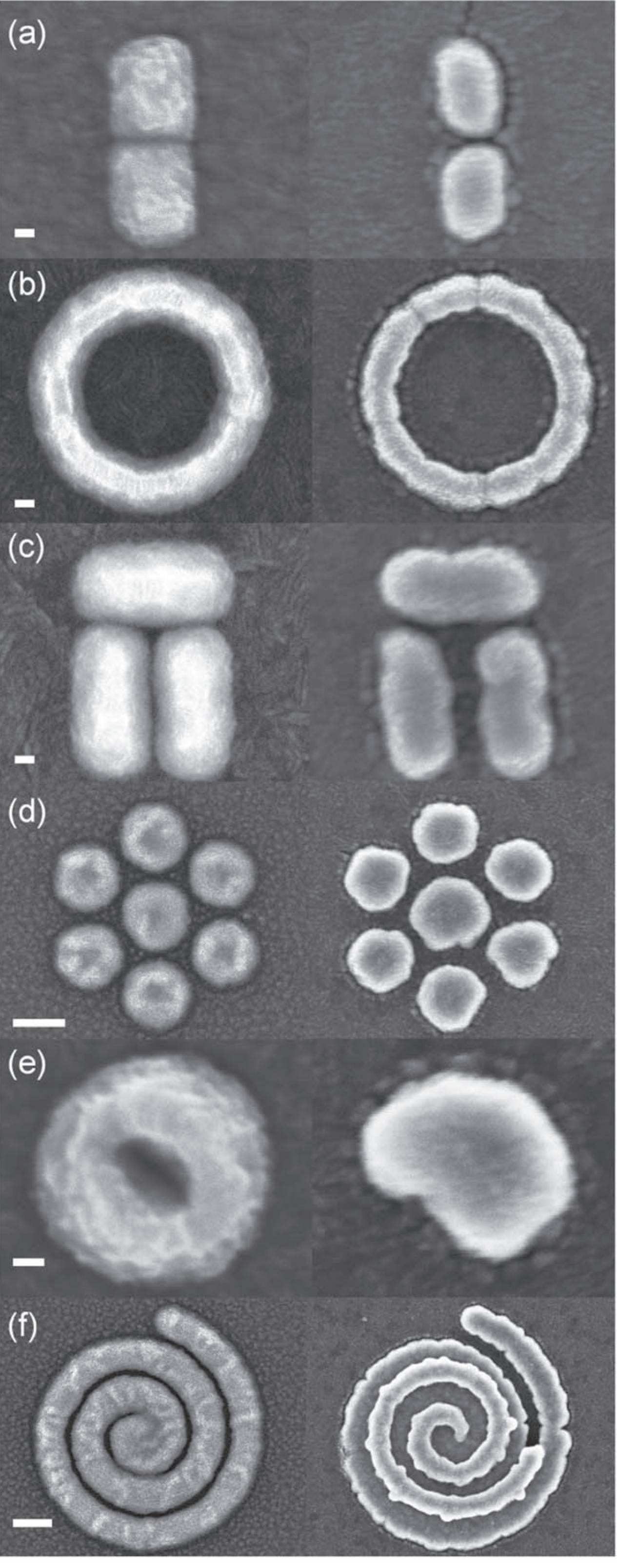

Figure 3. Comparison between plasmonic nanostructures fabricated by ion beam milling (left column) and lift-off (right column): (a) dipole antenna, (b) ring structure, (c) dolmen, (d) heptamer (e) doughnut and (f) spiral. Scale bars, (a), (b), (c), (e): 20 nm; (d) and (f): 100 nm.

and we are not limited by the grain formation after the evaporation onto the mask. Our aim is not to discuss here whether one structure would be 'better' than the other, but rather to draw attention to the fact that with the same e-beam writing, the resulting structures can be quite different, depending on the process used. This also emphasizes that the resolution is not solely determined by the e-beam. Finally, let us note that, due to the undercut, it is very difficult to fabricate nanostructures with voids using lift-off: the doughnut structure is rather ill-defined, figure 3(e), while the spiral is not properly opened, figure 3(f). In the latter panel, the low contrast object is the main spiral, while the brighter part is metal deposited on top of the remaining polymer (PMMA), which should have been removed by the lift-off process. Due to the very small gap and photoresist overexposure caused by the proximity of the exposed pixels, the lift-off was not successful in that case.

We resort to numerical simulations to study the influence of the fabricated nanostructures shapes on their optical response. Based on the SEM images shown in figure 4, we have built realistic finite elements models for some of the structures [72], and computed their response using the surface integral equation (SIE) [73, 74]. Contrary to volume methods [75], the SIE requires only the discretization of the scatterer surface. For the calculations shown in figure 4 a triangular mesh with average side of 8 nm was used to discretize the nanostructures surfaces, which were immersed in a homogeneous background with relative permittivity $\varepsilon = 1.625$ deduced from the average refractive index of the glass substrate and air (this simple approach mimics quite accurately the influence of a substrate on the plasmon resonance [76]). For the calculations, no residual HSQ was considered on top of the ion beam etched structures. Figure 4 shows the corresponding scattering cross sections, using the same arbitrary scale for all structures. While the spectra are different for ion beam milling and lift-off structures, it is interesting to note that the overall spectral response is maintained, also for the less accurate lift-off structures. For the dipole antenna in figure 4(a), we observe that the resonance for the ion beam structure is significantly red-shifted compared to that of the lift-off structure. This can be explained by the rounded structure [77], the shorter gap between both antenna arms [3, 8], and the residual HSQ on top [3]. Also, the quadrupolar resonance is visible as a shoulder in the spectrum of the ion beam structure. For the ring in figure 4(b) the lift-off structure is red-shifted compared to the ion beam etched one because the ring is thinner [78]. The dolmen structure in figure 4(c) exhibits multiple Fano resonances as dips around 700–800 nm and 900–1000 nm; such multiple features can occur in large dolmen structure [79], when the relative phase between the bright and dark modes changes [80]. The spectral feature around 700–800 nm is associated with the two vertical bars and is especially narrow for the ion beam structure [79]. The response of the heptamer in figure 4(d) also exhibits the signature of a Fano resonance around 750–800 nm [81]. It is

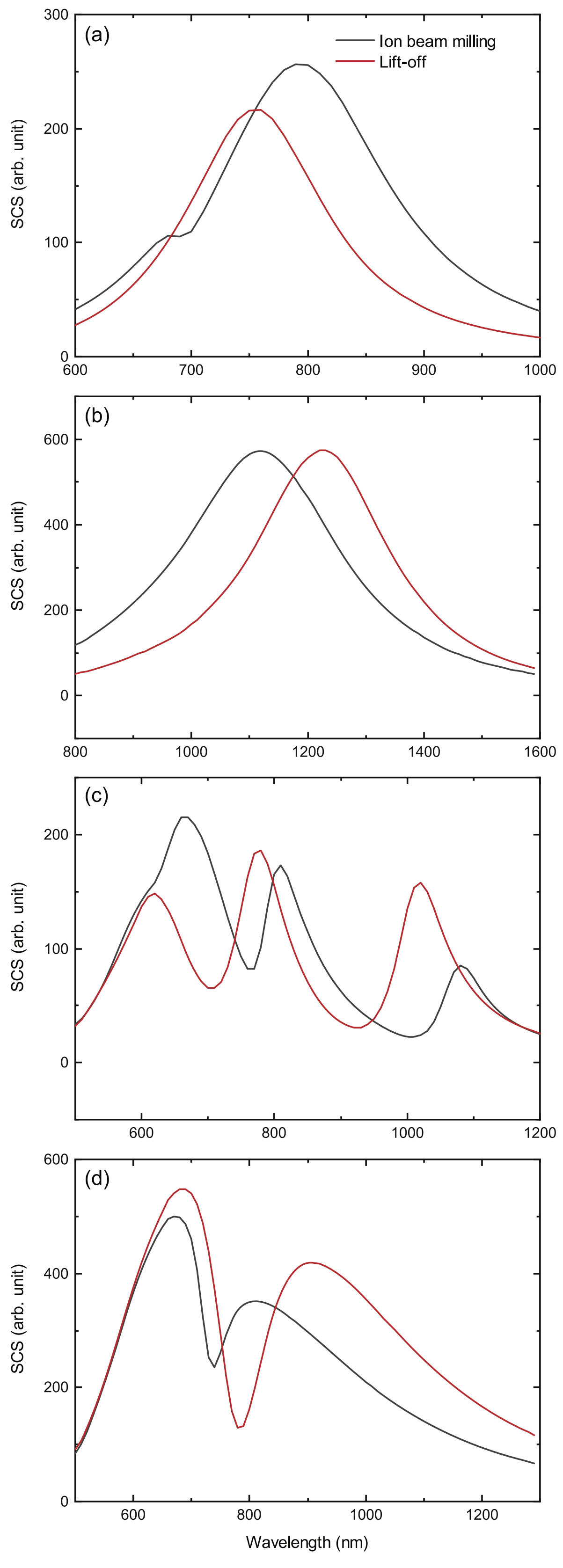

Figure 4. Calculations of the optical response for some of the structures fabricated in figure 3: (a) dipole antenna, (b) ring structure, (c) dolmen and (d) heptamer. The scattering cross section (SCS) is shown with the same arbitrary scale for all structures and discretized models based on the SEM images shown in figure 3 have been used for the calculations.

interesting to note that for this geometry, the extremely tight structure obtained by ion etching has a less prominent Fano dip, compared to the more irregular structure obtained by lift-off, which is in agreement with results from Hetschel *et al* [82].

In summary, we have detailed two different approaches for the fabrication of metallic nanostructures based on e-beam lithography. The first approach relies on a negative e-beam resist, followed with ion beam milling, while the second uses a positive e-beam resist and lift-off. Overall, ion beam etching provides smaller and more regular features, that can be controlled down to about 10 nm. In the lift-off process, the metal atoms are deposited within the e-beam resist mask and can diffuse on the substrate, rendering the nanostructure outline slightly fuzzy. Comparing the scattering cross sections computed for both approaches, we observed quite some spectral differences related to the overall size of the structures (usually the lift-off structures are larger than the ion beam milled ones) or to some specific geometrical details. These differences are especially visible for structures that support complex resonances, such as Fano resonances. Both approaches can produce useful nanostructures and the results reported therein should guide the researcher to choose the best suited approach for a given application, depending on the available technology.

Acknowledgments

Funding from the European Research Council (ERC-2015-AdG-695206 Nanofactory) and from the Swiss National Science Foundation (Project 200 020_135452) is gratefully acknowledged.

Data availability statement

The data that support the findings of this study are openly available at the following URL/DOI:http://doi.org/10.5281/zenodo.5011466.

ORCID iDs

B Abasahl https://orcid.org/0000-0001-5618-4572
C Santschi https://orcid.org/0000-0001-9830-3904
T V Raziman https://orcid.org/0000-0002-7085-6934
O J F Martin https://orcid.org/0000-0002-9574-3119

References

[1] Stockman M I 2011 Nanoplasmonics: past, present, and glimpse into future *Opt. Express* **19** 22029–106
[2] Kottmann J P, Martin O J F, Smith D R and Schultz S 2000 Field polarization and polarization charge distributions in plasmon resonant nanoparticles *New J. Phys.* **2** 27–27

[3] Fischer H and Martin O J F 2008 Engineering the optical response of plasmonic nanoantennas *Opt. Express* **16** 9144–54
[4] Ciracì C, Hill R T, Mock J J, Urzhumov Y, Fernández-Domínguez A I, Maier S A, Pendry J B, Chilkoti A and Smith D R 2012 Probing the ultimate limits of plasmonic enhancement *Science* **337** 1072–4
[5] Hill R T, Mock J J, Hucknall A, Wolter S D, Jokerst N M, Smith D R and Chilkoti A 2012 Plasmon ruler with angstrom length resolution *ACS Nano* **6** 9237–46
[6] Sigle D O, Zhang L, Ithurria S, Dubertret B and Baumberg J J 2015 Ultrathin cdse in plasmonic nanogaps for enhanced photocatalytic water splitting *J. Phys. Chem. Lett.* **6** 1099–103
[7] Chikkaraddy R, de Nijs B, Benz F, Barrow S J, Scherman O A, Rosta E, Demetriadou A, Fox P, Hess O and Baumberg J J 2016 Single-molecule strong coupling at room temperature in plasmonic nanocavities *Nature* **535** 127–30
[8] Zuloaga J, Prodan E and Nordlander P 2009 Quantum description of the plasmon resonances of a nanoparticle dimer *Nano Lett.* **9** 887–91
[9] Savage K J, Hawkeye M M, Esteban R, Borisov A G, Aizpurua J and Baumberg J J 2012 Revealing the quantum regime in tunnelling plasmonics *Nature* **491** 574–7
[10] Liz-Marzán L M 2006 Tailoring surface plasmons through the morphology and assembly of metal nanoparticles *Langmuir* **22** 32–41
[11] Rycenga M, Cobley C M, Zeng J, Li W, Moran C H, Zhang Q, Qin D and Xia Y 2011 Controlling the synthesis and assembly of silver nanostructures for plasmonic applications *Chem. Rev.* **111** 3669–712
[12] Tan S J, Campolongo M J, Luo D and Cheng W 2011 Building plasmonic nanostructures with DNA *Nat. Nanotechnol.* **6** 268–76
[13] Saha K, Agasti S S, Kim C, Li X N and Rotello V M 2012 Gold nanoparticles in chemical and biological sensing *Chem. Rev.* **112** 2739–79
[14] Craighead H G and Niklasson G A 1984 Characterization and optical properties of arrays of small gold particles *Appl. Phys. Lett.* **44** 1134–6
[15] Krenn J R, Gotschy W, Somitsch D, Leitner A and Aussenegg F R 1995 Investigation of localized surface-plasmons with the photon scanning tunneling microscope *Appl. Phys.* A **61** 541–5
[16] Weeber J-C, Bourillot E, Dereux A, Goudonnet J-P, Chen Y and Girard C 1996 Observation of light confinement effects with a near-field optical microscope *Phys. Rev. Lett.* **77** 5332–5
[17] Gotschy W, Vonmetz K, Leitner A and Aussenegg F R 1996 Thin films by regular patterns of metal nanoparticles: tailoring the optical properties by nanodesign *Appl. Phys.* B **63** 381–4
[18] Weeber J C, Girard C, Krenn J R, Dereux A and Goudonnet J P 1999 Near-field optical properties of localized plasmons around lithographically designed nanostructures *J. Appl. Phys.* **86** 2576–83
[19] Bozhevolnyi S I, Erland J, Leosson K, Skovgaard P M W and Hvam J M 2001 Waveguiding in surface plasmon polariton band gap structures *Phys. Rev. Lett.* **86** 3008–11
[20] Nikolajsen T, Leosson K and Bozhevolnyi S I 2004 Surface plasmon polariton based modulators and switches operating at telecom wavelengths *Appl. Phys. Lett.* **85** 5833
[21] Charbonneau R, Lahoud N, Mattiussi G and Berini P 2005 Demonstration of integrated optics elements based on long-ranging surface plasmon polaritons *Opt. Express* **13** 977–84
[22] Liu N, Guo H, Fu L, Kaiser S, Schweizer H and Giessen H 2008 Three-dimensional photonic metamaterials at optical frequencies *Nat. Mater.* **7** 31–7
[23] Lereu A L, Sanchez-Mosteiro G, Ghenuche P, Quidant R and van Hulst N F 2008 Individual gold dimers investigated by far- and near-field imaging *J. Microsc.* **229** 254–8
[24] Huang L, Maerkl S and Martin O J F 2009 Integration of plasmonic trapping in a microfluidic environment *Opt. Express* **17** 6018–24
[25] Yu N, Genevet P, Kats M A, Aieta F, Tetienne J-P, Capasso F and Gaburro Z 2011 Light propagation with phase discontinuities: generalized laws of reflection and refraction *Science* **334** 333–7
[26] Berini P and De Leon I 2012 Surface plasmon-polariton amplifiers and lasers *Nat. Photon.* **6** 16–24
[27] Cinel N A, Bütün S and Özbay E 2012 Electron beam lithography designed silver nano-disks used as label free nano-biosensors based on localized surface plasmon resonance *Opt. Express* **20** 2587–97
[28] Paolo B, Jer-Shing H and Bert H 2012 Nanoantennas for visible and infrared radiation *Rep. Prog. Phys.* **75** 024402
[29] Lovera A, Gallinet B, Nordlander P and Martin O J F 2013 Mechanisms of fano resonances in coupled plasmonic systems *ACS Nano* **7** 4527–36
[30] Lu B-R, Deng J, Li Q, Zhang S, Zhou J, Zhou L and Chen Y 2018 Reconstructing a plasmonic metasurface for a broadband high-efficiency optical vortex in the visible frequency *Nanoscale* **10** 12378–85
[31] Cetin A E, Yilmaz C, Galarreta B C, Yilmaz G, Altug H and Busnaina A 2020 Fabrication of sub-10-nm plasmonic gaps for ultra-sensitive raman spectroscopy *Plasmonics* **15** 1165–71
[32] Kurihara K, Rockstuhl C, Petit S, Yamakawa Y and Tominaga J 2008 Plasmonic devices with controllable resonances—an avenue towards high-speed and mass fabrication of optical meta-materials *J. Microsc.* **229** 396–401
[33] Siegfried T, Wang L, Ekinci Y, Martin O J F and Sigg H 2014 Metal double layers with sub-10 nm channels *ACS Nano* **8** 3700–6
[34] Sun L *et al* 2016 High throughput fabrication of large-area plasmonic color filters by soft-x-ray interference lithography *Opt. Express* **24** 19112–21
[35] Boltasseva A 2009 Plasmonic components fabrication via nanoimprint *J. Opt. A: Pure Appl. Opt.* **11** 114001
[36] Liang C-C, Liao M-Y, Chen W-Y, Cheng T-C, Chang W-H and Lin C-H 2011 Plasmonic metallic nanostructures by direct nanoimprinting of gold nanoparticles *Opt. Express* **19** 4768–76
[37] Svavarsson H G, Yoon J W, Song S H and Magnusson R 2011 Fabrication of large plasmonic arrays of gold nanocups using inverse periodic templates *Plasmonics* **6** 741
[38] Vazquez-Mena O, Sannomiya T, Tosun M, Villanueva L G, Savu V, Voros J and Brugger J 2012 High-resolution resistless nanopatterning on polymer and flexible substrates for plasmonic biosensing using stencil masks *ACS Nano* **6** 5474–81
[39] Liu F, Luber E J, Huck L A, Olsen B C and Buriak J M 2015 Nanoscale plasmonic stamp lithography on silicon *ACS Nano* **9** 2184–93
[40] Kim J *et al* 2021 Fabrication of plasmonic arrays of nanodisks and nanotriangles by nanotip indentation lithography and their optical properties *Nanoscale* **13** 4475–84
[41] Fischer U C and Zingsheim H P 1981 Submicroscopic pattern replication with visible light *J. Vac. Sci. Technol.* **19** 881–5
[42] Junesch J, Sannomiya T and Dahlin A B 2012 Optical properties of nanohole arrays in metal-dielectric double films prepared by mask-on-metal colloidal lithography *ACS Nano* **6** 10405–15
[43] Bochenkov V E and Sutherland D S 2013 From rings to crescents: a novel fabrication technique uncovers the transition details *Nano Lett.* **13** 1216–20

[44] Shi G C, Wang M L, Zhu Y Y, Yan X Y, Pan S Y and Zhang A Q 2019 Nanoflower-like Ag/AAO SERS platform with quasi-photonic crystal nanostructure for efficient detection of goat serum *Curr. Appl. Phys.* **19** 1276–85
[45] Thangamuthu M, Santschi C and Martin O J F 2020 Reliable langmuir blodgett colloidal masks for large area nanostructure realization *Thin Solid Films* **709** 138195
[46] Devaux E, Ebbesen T W, Weeber J C and Dereux A 2003 Launching and decoupling surface plasmons via micro-gratings *Appl. Phys. Lett.* **83** 4936
[47] Nomura W, Ohtsu M and Yatsui T 2005 Nanodot coupler with a surface plasmon polariton condenser for optical far/near-field conversion *Appl. Phys. Lett.* **86** 181108
[48] Muhlschlegel P, Eisler H-J, Martin O J F, Hecht B and Pohl D W 2005 Resonant optical antennas *Science* **308** 1607–8
[49] Dhawan A, Gerhold M, Madison A, Fowlkes J, Russell P E, Vo-Dinh T and Leonard D N 2009 Fabrication of nanodot plasmonic waveguide structures using fib milling and electron beam-induced deposition *Scanning* **31** 139–46
[50] Santschi C, Przybylska J, Guillaumee M, Vazquez-Men O, Brugger J and Martin O J F 2009 Focused ion beam: a versatile technique for the fabrication of nano-devices *Pract. Metallogr.* **46** 154–6
[51] Ou J-Y, Plum E, Zhang J and Zheludev N I 2013 An electromechanically reconfigurable plasmonic metamaterial operating in the near-infrared *Nat. Nanotechnol.* **8** 252–5
[52] Huang J S, Feichtner T, Biagioni P and Hecht B 2009 Impedance matching and emission properties of nanoantennas in an optical nanocircuit *Nano Lett.* **9** 1897–902
[53] Huang J-S *et al* 2010 Atomically flat single-crystalline gold nanostructures for plasmonic nanocircuitry *Nat. Commun.* **1** 150
[54] Kern J, Großmann S, Tarakina N V, Häckel T, Emmerling M, Kamp M, Huang J-S, Biagioni P, Prangsma J C and Hecht B 2012 Atomic-scale confinement of resonant optical fields *Nano Lett.* **12** 5504–9
[55] Chen K, Razinskas G, Feichtner T, Grossmann S, Christiansen S and Hecht B 2016 Electromechanically tunable suspended optical nanoantenna *Nano Lett.* **16** 2680–5
[56] Boroviks S, Todisco F, Mortensen N A and Bozhevolnyi S I 2019 Use of monocrystalline gold flakes for gap plasmon-based metasurfaces operating in the visible *Opt. Mater. Express* **9** 4209–17
[57] Kumar S, Leissner T, Boroviks S, Andersen S K H, Fiutowski J, Rubahn H G, Mortensen N A and Bozhevolnyi S I 2020 Efficient coupling of single organic molecules to channel plasmon polaritons supported by V-grooves in monocrystalline gold *Acs Photon.* **7** 2211–8
[58] Murray W A and Barnes W L 2007 Plasmonic materials *Adv. Mater.* **19** 3771–82
[59] West P R, Ishii S, Naik G V, Emani N K, Shalaev V M and Boltasseva A 2010 Searching for better plasmonic materials *Laser Photon. Rev.* **4** 795–808
[60] Babicheva V E, Kinsey N, Naik G V, Ferrera M, Lavrinenko A V, Shalaev V M and Boltasseva A 2013 Towards cmos-compatible nanophotonics: ultra-compact modulators using alternative plasmonic materials *Opt. Express* **21** 27326–37
[61] Naik G V, Shalaev V M and Boltasseva A 2013 Alternative plasmonic materials: beyond gold and silver *Adv. Mater.* **25** 3264–94
[62] Thyagarajan K, Santschi C, Langlet P and Martin O J F 2016 Highly improved fabrication of Ag and Al nanostructures for UV and nonlinear plasmonics *Adv. Opt. Mater.* **4** 871–6
[63] Méjard R, Verdy A, Demichel O, Petit M, Markey L, Herbst F, Chassagnon R, Colas-des Francs G, Cluzel B and Bouhelier A 2017 Advanced engineering of single-crystal gold nanoantennas *Opt. Mater. Express* **7** 1157–68
[64] Ray D, Raziman T V, Santschi C, Etezadi D, Altug H and Martin O J F 2020 Hybrid metal-dielectric metasurfaces for refractive index sensing *Nano Lett.* **20** 8752–9
[65] Jiao X, Goeckeritz J, Blair S and Oldham M 2009 Localization of near-field resonances in bowtie antennae: influence of adhesion layers *Plasmonics* **4** 37–50
[66] Siegfried T, Ekinci Y, Martin O J F and Sigg H 2013 Engineering metal adhesion layers that do not deteriorate plasmon resonances *ACS Nano* **7** 2751–7
[67] Wang X, Santschi C and Martin O J F 2017 Strong improvement of long-term chemical and thermal stability of plasmonic silver nanoantennas and films *Small* **13** 1700044
[68] Alam A U, Howlader M M R and Deen M J 2013 Oxygen plasma and humidity dependent surface analysis of silicon, silicon dioxide and glass for direct wafer bonding *ECS J. Solid State Sci. Technol.* **2** P515–23
[69] Alam A U, Howlader M M R and Deen M J 2014 The effects of oxygen plasma and humidity on surface roughness, water contact angle and hardness of silicon, silicon dioxide and glass *J. Micromech. Microeng.* **24** 14
[70] Abe H, Yoneda M and Fujlwara N 2008 Developments of plasma etching technology for fabricating semiconductor devices *Japan. J. Appl. Phys.* **47** 1435–55
[71] Wu B Q, Kumar A and Pamarthy S 2010 High aspect ratio silicon etch: a review *J. Appl. Phys.* **108** 051101
[72] Kern A M and Martin O J F 2011 Excitation and reemission of molecules near realistic plasmonic nanostructures *Nano Lett.* **11** 482–7
[73] Kern A M and Martin O J F 2009 Surface integral formulation for 3d simulations of plasmonic and high permittivity nanostructures *J. Opt. Soc. Am.* A **26** 732–40
[74] Raziman T V, Somerville W R C, Martin O J F and Le Ru E C 2015 Accuracy of surface integral equation matrix elements in plasmonic calculations *J. Opt. Soc. Am.* B **32** 485–92
[75] Martin O J F and Piller N B 1998 Electromagnetic scattering in polarizable backgrounds *Phys. Rev.* E **58** 3909–15
[76] Gay-Balmaz P and Martin O J F 2001 Electromagnetic scattering of high-permittivity particles on a substrate *Appl. Opt.* **40** 4562–9
[77] Raziman T V and Martin O J F 2013 Polarisation charges and scattering behaviour of realistically rounded plasmonic nanostructures *Opt. Express* **21** 21500–7
[78] Aizpurua J, Hanarp P, Sutherland D S, Käll M, Bryant G W and García de Abajo F J 2003 Optical properties of gold nanorings *Phys. Rev. Lett.* **90** 057401
[79] Verellen N, Sonnefraud Y, Sobhani H, Hao F, Moshchalkov V V, Van Dorpe P, Nordlander P and Maier S A 2009 Fano resonances in individual coherent plasmonic nanocavities *Nano Lett.* **9** 1663–7
[80] Gallinet B and Martin O J F 2011 Relation between near-field and far-field properties of plasmonic fano resonances *Opt. Express* **19** 22167–75
[81] Fan J A, Wu C, Bao K, Bao J, Bardhan R, Halas N J, Manoharan V N, Nordlander P, Shvets G and Capasso F 2010 Self-assembled plasmonic nanoparticle clusters *Science* **328** 1135–8
[82] Hentschel M, Saliba M, Vogelgesang R, Giessen H, Alivisatos A P and Liu N 2010 Transition from isolated to collective modes in plasmonic oligomers *Nano Lett.* **10** 2721–6